Multi-Neutrino Entanglement and Correlations in Dense Neutrino Systems

Marc Illa* and Martin J. Savage†
InQubator for Quantum Simulation (IQuS), Department of Physics, University of Washington, Seattle, Washington 98195, USA

(Received 7 December 2022; revised 27 April 2023; accepted 28 April 2023; published 31 May 2023)

The time evolution of multi-neutrino entanglement and correlations are studied in two-flavor collective neutrino oscillations, relevant for dense neutrino environments, building upon previous works. Specifically, simulations performed of systems with up to 12 neutrinos using Quantinuum's `H1-1` 20 qubit trapped-ion quantum computer are used to compute n-tangles, and two- and three-body correlations, probing beyond mean-field descriptions. n-tangle rescalings are found to converge for large system sizes, signaling the presence of genuine multi-neutrino entanglement.

DOI: 10.1103/PhysRevLett.130.221003

In extreme astrophysical environments, such as those found in core-collapse supernovae, neutrino densities are sufficiently high to participate in the transport of energy and momentum, in local chemical compositions and in dynamics [1–5]. Coherent evolution of lepton flavors, that depends on self-interactions between neutrinos induced by weak interactions [6–10], plays an important role. First studies of the quantum correlations in coherent evolution of dense neutrino systems, beyond mean-field descriptions, are providing important insights into such dynamics [11–28]. So far, they have focused on bipartite entanglement witnesses, such as entanglement entropy, negativity, and concurrence [15–19,21–26]. In this work, we explore multi-neutrino entanglement in such systems by computing n-tangles [29], τ_n, between n neutrinos induced by time evolution. The total n-tangles at late times are found to scale for large system sizes. Our work utilized classical simulations, and quantum simulations using the Quantinuum 20-qubit trapped-ion quantum computer `H1-1` and noisy emulator `H1-1E` [30].

The leading-order low-energy effective Hamiltonian describing collective, coherent neutrino flavor oscillations is composed of three terms. One term is responsible for vacuum oscillations, originating from the neutrino mass matrix [31–34]. A second is from the weak interactions between neutrinos and matter, mainly between ν_e and e^-, through charged-current processes, and is responsible for the Mikheev-Smirnov-Wolfenstein effect [35,36]. In what follows, we neglect the contributions from this term. A third term, from the neutral-current weak interactions, is responsible for coherent forward scattering of neutrinos, which becomes significant at sufficiently high neutrino densities [7–10].

Because of the small value of θ_{13} [37], three-flavor neutrino systems can be approximated by two-flavor systems involving the electron neutrino ν_e and a heavy neutrino ν_x, considered to be a combination of ν_μ and ν_τ [38]. The effective Hamiltonian for N neutrinos can be written in terms of spin operators acting in flavor space [14],

$$H = H^{\nu} + H^{\nu\nu} = \sum_i \mathbf{b}\cdot\boldsymbol{\sigma}^{(i)} + \frac{1}{N}\sum_{i<j} J_{ij}\boldsymbol{\sigma}^{(i)}\cdot\boldsymbol{\sigma}^{(j)}, \quad (1)$$

where $\boldsymbol{\sigma}^{(i)} = (\sigma_x^{(i)}, \sigma_y^{(i)}, \sigma_z^{(i)})$ are the Pauli matrices acting on the ith neutrino flavor doublet $(|\nu_e\rangle, |\nu_x\rangle)^T$. The three-vector $\mathbf{b}$ encodes the vacuum oscillations,

$$\mathbf{b} = \frac{\Delta m^2}{4E}[\sin(2\theta_v), 0, -\cos(2\theta_v)], \quad (2)$$

with Δm^2 being the difference between neutrino squared masses, E the neutrino energy, and θ_v the vacuum-mixing angle. The two-body couplings J_{ij}, uniquely defined at leading order by the standard model, are

$$J_{ij} = \sqrt{2}G_F\rho_\nu(1-\cos\theta_{ij}), \quad (3)$$

where G_F is Fermi's constant, ρ_ν the number-density of neutrinos, and θ_{ij} the angle of the momenta between the ith and jth neutrino. Following previous works, e.g., Refs. [18,28], we introduce $\mu \equiv \sqrt{2}G_F\rho_\nu$, and, for demonstrative purposes, set $\mu/N = \Delta m^2/4E$ (assuming a monochromatic beam), so that the one- and two-body terms have comparable strengths [18]. Following the inspiring work of Hall *et al.* [18], a one-parameter set is used to demonstrate relevant physics, with a vacuum-mixing angle of $\theta_v = 0.195$, a distribution of momenta with $\theta_{ij} = \arccos(0.9)\times|i-j|/(N-1)$ (cone-shaped), and an initial state that is a product state of $N/2|\nu_e\rangle$ and $N/2|\nu_x\rangle$, i.e., $|\Psi_0\rangle = |\nu_e\rangle^{\otimes N/2}\otimes|\nu_x\rangle^{\otimes N/2}$.

While a number of previous calculations of neutrino systems using quantum devices have been focused on the coherent time evolution of the flavor content [18,20,25,28], and the entanglement of one or two neutrinos [18,25], here we examine correlations between different neutrinos and multibody entanglement, quantities that can further probe mean-field descriptions of these systems. Specifically, we

look at the two-body correlations, as considered previously, e.g., Ref. [26],

$$\mathcal{C}_{ij}^{(2\nu)}(t) = \langle \sigma_z^{(i)} \sigma_z^{(j)} \rangle - \langle \sigma_z^{(i)} \rangle \langle \sigma_z^{(j)} \rangle, \qquad i \neq j, \tag{4}$$

with $\langle \cdot \rangle = \langle \Psi_t | \cdot | \Psi_t \rangle$, and three-body correlations,

$$\begin{aligned} \mathcal{C}_{ijk}^{(3\nu)}(t) = & \langle \sigma_z^{(i)} \sigma_z^{(j)} \sigma_z^{(k)} \rangle - \langle \sigma_z^{(i)} \rangle \langle \sigma_z^{(j)} \sigma_z^{(k)} \rangle \\ & - \langle \sigma_z^{(j)} \rangle \langle \sigma_z^{(i)} \sigma_z^{(k)} \rangle - \langle \sigma_z^{(k)} \rangle \langle \sigma_z^{(i)} \sigma_z^{(j)} \rangle \\ & + 2 \langle \sigma_z^{(i)} \rangle \langle \sigma_z^{(j)} \rangle \langle \sigma_z^{(k)} \rangle, \qquad i \neq j \neq k. \end{aligned} \tag{5}$$

Ultimately, studies of entanglement will help quantify the limitations of classical techniques in providing reliable and accurate results, and can also guide tensor-networks approaches [17,19,24]. Entanglement in neutrino systems has been previously computed via full-state tomography [18,25], which, however, is expected to become inefficient for larger systems due to the required number of measurements. Alternative methods including classical shadows [39], which are expected to require fewer measurements, are currently being pursued.

As a way to gain further insight into the entanglement structure of dense, coherent neutrino systems, we focus on the n-tangle τ_n, defined as $|\langle \Psi | \sigma_y^{\otimes n} | \Psi^* \rangle|^2$, where $|\Psi^*\rangle$ is the complex conjugate of $|\Psi\rangle$. This quantity is a measure of the n-body entanglement [29]. For two-qubit (neutrino) systems, τ_2 is the concurrence squared [40,41], C_{12}^2. For three-qubit systems, τ_3 is the residual entanglement [42], $C_{1(23)}^2 - C_{12}^2 - C_{13}^2$, with $C_{1(23)} = \sqrt{2 - 2\mathrm{Tr}\rho_1^2}$, with ρ_1 the reduced density matrix of the first qubit. However, for $n \geq 4$, τ_n is not uniquely the residual entanglement, and it is smaller than or equal to the concurrence $C_{1(2\ldots n)}$ [43]. An interesting property of τ_n is that, for the N-qubit GHZ state [44,45], $\tau_N = 1$, while for the N-qubit W state [46], $\tau_N = 0$. Thus, while it can help distinguish between different types of entanglement, by itself it is not a measure of N-body entanglement [29,47].

Implementation on a quantum computer.—Previous works have performed quantum simulations of these systems using IBM's superconducting-qubit quantum computers [18,20], D-Wave's superconducting-qubit annealing devices [25] and Quantinuum's Trapped-ion quantum computers [28]. We implement the time evolution of an initial state Ψ_0 under the Hamiltonian given in Eq. (1) using Quantinuum's `H1-1` 20 qubit trapped-ion quantum computer, that is based on using the two hyperfine clock states in the $^2S_{1/2}$ ground state of $^{172}Yb^+$ ions as qubits [30]. For purposes of comparison, we also provide results obtained using its emulator, `H1-1E` (Ref. [50] showed that `H1-1E` could well reproduce the behavior of `H1-1`). The evolution operator, $\exp(-itH)$, is Trotterized, and each contribution is mapped to a quantum circuit composed of gates that are native to `H1-1`. As noted in Ref. [28], the one-body and two-body parts of the Hamiltonian commute, $[H^\nu, H^{\nu\nu}] = 0$, so they can be Trotterized without introducing a higher-order systematic error. For H^ν, since each term acts on a different neutrino,

$$e^{-itH^\nu} = \bigotimes_i e^{-it\mathbf{b}\cdot\boldsymbol{\sigma}^{(i)}}. \tag{6}$$

This term is implemented with the following Euler decomposition for SU(2) matrices [51],

$$e^{-it\mathbf{b}\cdot\boldsymbol{\sigma}^{(i)}} = \quad -\boxed{R_z(\alpha_1)}-\boxed{R_y(\alpha_2)}-\boxed{R_z(\alpha_3)}-, \tag{7}$$

where the angles α_i are fixed numerically.

For $H^{\nu\nu}$, the known decomposition of SU(4) matrices with 3 CNOT gates [52] is used,

$$e^{-itJ_{ij}\boldsymbol{\sigma}^{(i)}\cdot\boldsymbol{\sigma}^{(j)}} =$$

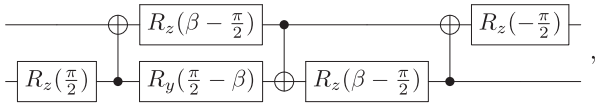

, (8)

with $\beta = 2tJ_{ij}$, which has a slight advantage over [53,54] (requiring 5 single-qubits gates instead of 8). While not directly relevant to the present set of simulation, it is interesting to consider the T-gate resource requirements for such simulation. Standard methods [55] suggest a T-gate count of $N(187N - 101)/2$ for $\epsilon = 10^{-4}$, for N neutrinos per Trotter step. While the circuits in Eqs. (7) and (8) are not written in terms of the native gates used in `H1-1` (these can be found in Ref. [28]), the package PYTKET [60] includes a function that performs this translation, along with optimizations. Implementation of this two-neutrino term is more delicate. Since the sum over different pairs of neutrinos is split in the implementation of the time-evolution operator, the noncommutativity of terms introduces systematic Trotter errors. While it is possible to find a combination that minimizes this error, as in Ref. [28] for the case of 4 neutrinos, this is not feasible for larger systems. As shown in Ref. [18], it is possible to build a circuit that performs the Trotterized version of $\exp(-itH^{\nu\nu})$ with N layers of the operator in Eq. (8) (if multiple gates can be applied in parallel across the device). Figure 1 shows the circuits used for different number of neutrinos. A nice property of these circuits is that they retain the symmetry present in the Hamiltonian given in Eq. (1), between the exchange of the ith and $(N - i + 1)$th neutrino, for the current choice of J_{ij}. While first order Trotter evolution has been used, higher orders with their improved convergence have been explored in Ref. [28]. They found that the Trotter errors from first and second order evolution from the prepared initial state are significantly smaller than naive theoretical bounds. Alternative methods for time evolution,

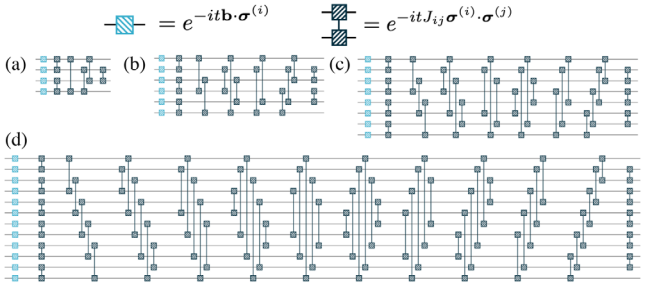

FIG. 1. Circuits for a single Trotter step for (a) $N = 4$, (b) $N = 6$, (c) $N = 8$, and (d) $N = 12$ neutrinos, where the two-neutrino gates are clustered into groups that can be applied in parallel, showing the linear scaling with N of the circuit depth.

such as variational fast forwarding [61], should also be examined.

Two- and three-neutrino correlations.—A term that appears in the computation of correlation functions is the expectation value of σ_z. For this reason, it is interesting to first compute the inversion probability for a single neutrino, defined as

$$P_i(t) = \frac{1}{2}(1 \mp \langle \sigma_z^{(i)} \rangle), \tag{9}$$

where the $\mp$ sign depends on the initial state of the ith neutrino ($-$ for ν_e and $+$ for ν_x). Because of the symmetry of the Hamiltonian (and its Trotterized version), the inversion probabilities for the ith and $(N - i + 1)$th neutrino are the same. The results for $N = 12$ are shown in Fig. 2, where the two icons in the legend indicate whether a quantum device (blue) or emulator (yellow) was used to obtain the results [62], and the $N = 8$ are in the Supplemental Material [63]. The uncertainties in the results are computed via bootstrap resampling. For the $N = 8$ case, agreement is found with the results presented in Ref. [28].

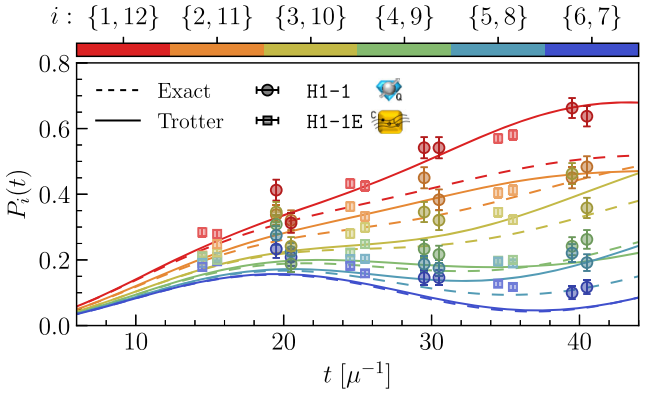

FIG. 2. Flavor inversion probabilities for $N = 12$ neutrinos. The lines show the single-step Trotter (continuous) and exact (dashed) simulations, and the points show the results from `H1-1` (dark circles, using 240 shots) and `H1-1E` (light squares, using 1200 shots).

For $N = 12$, both results from `H1-1` and `H1-1E` are showing somewhat larger deviations from expectations, but the device has remained coherent (the associated Supplemental Material [63] gives the numerical values of the results shown in Fig. 2, and those shown in subsequent figures).

As a selection of two- and three-body correlations, we focus on

$$\mathcal{C}_{1i}^{(2\nu)}, \quad \text{with} \quad 1 < i \leq N, \qquad \mathcal{C}_{1iN}^{(2\nu)}, \quad \text{with} \quad 1 < i < N,$$
$$\mathcal{C}_{i,i+1}^{(2\nu)}, \quad \text{with} \quad 1 \leq i < N, \qquad \mathcal{C}_{i-1,i,i+1}^{(3\nu)}, \quad \text{with} \quad 1 < i < N.$$

A representative set of correlation functions for $N = 12$ neutrinos is shown in Fig. 3, and a more complete set can be found in the Supplemental Material [63]. For the two-body correlations, results from `H1-1` and `H1-1E` follow the expected values, although somewhat limited by statistics. This gets more prominent when looking at the three-body correlations, where with the current uncertainties most of the points are consistent with zero. As seen by comparing the results from `H1-1` and `H1-1E`, increasing the accumulated statistics by factor of 5 makes a substantial difference, but it remains insufficient. Increasing further the number of shots would help resolve those small values, which would be reasonable with, for instance, IBM's quantum computers (where usually one works with $\gtrsim 10^4$ shots). With the possibility of performing more shots, error mitigation techniques, such as randomized compiling [64] and decoherence renormalization [65–67], become viable. While these correlations differ from zero, with a hierarchy $\mathcal{C}^{(2\nu)} > \mathcal{C}^{(3\nu)}$, an interesting trend is that $\mathcal{C}_{1i}^{(2\nu)}$ plateaus at late times, with $\mathcal{C}_{12}^{(2\nu)}$ reaching a value ~ 0.5, down to ~ -0.5 for $\mathcal{C}_{1N}^{(2\nu)}$. Other limiting patterns are not found for other computed quantities.

A potential improvement to the current results has been explored, in which a postselection of the counts that satisfy the symmetries of the Hamiltonian. This technique has been used with great success when studying quantum field theories, e.g., see Refs. [50,67–69]. However, specific to this system in the flavor basis, $\mathbf{b} \cdot \mathbf{J}$ is the conserved quantity (and not J_z), which makes postselection not feasible in our studies (calculations could be performed in the mass basis, but the selected initial state would then be a sum of product states, which would complicate the calculation of the n-tangle).

Multi-neutrino entanglement.—The N-tangle, τ_N, is an interesting measure of multi-neutrino entanglement in these systems, which is straightforward to compute via

$$\tau_N(t) = |\langle \Psi_t | \sigma_y^{\otimes N} | \Psi_t^* \rangle|^2 = |\langle \Psi_0 | e^{itH} \sigma_y^{\otimes N} e^{itH} | \Psi_0 \rangle|^2, \tag{10}$$

(without the need to use the SWAP test [70–72] to compute the overlap). We have performed such calculations for the system of $N = 4$ neutrinos using `H1-1` and `H1-1E`, as

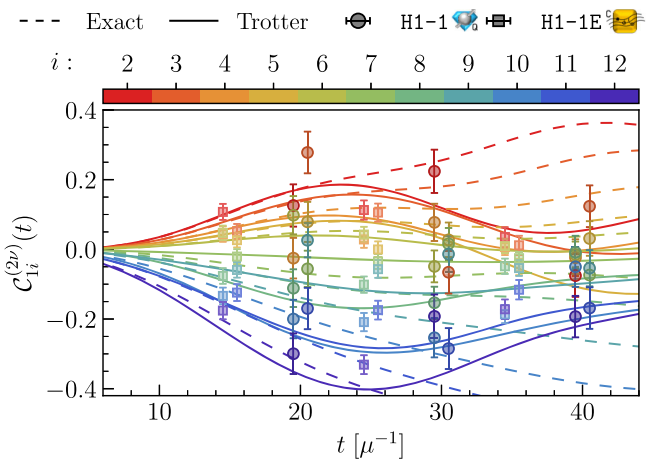

FIG. 3. Two-body correlation for $N = 12$ neutrinos. The lines show the single-step Trotter (continuous) or exact (dashed) simulation, and the points show the results from `H1-1` (dark circles, using 240 shots) and `H1-1E` (light squares, using 1200 shots).

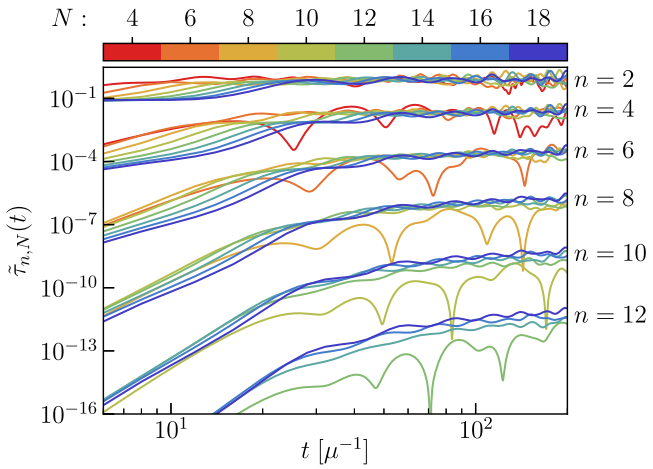

FIG. 5. The rescaled n-tangle, $\tilde{\tau}_{n,N}$, defined in Eq. (11), for $n = \{2, \ldots, 12\}$ and $N = \{4, \ldots, 18\}$ neutrinos.

shown in the top panel of Fig. 4, where two Trotter steps have been used in applying e^{itH}. The $N = 6$ system has also been studied, but only using `H1-1E` (and with a single Trotter step). For the time-range displayed, τ_N is seen to decrease rapidly with system size.

To further explore the dependence of multi-neutrino entanglement with system size, it is interesting to look at τ_n, with $n < N$. For this quantity, a rescaling of the sum of the τ_ns is found to be helpful,

$$\tilde{\tau}_{n,N} = \frac{1}{N^{n-2}} \sum_i \tau_n^{(i)}, \tag{11}$$

where the index i in $\tau_n^{(i)}$ identifies one of the possible $\binom{N}{n}$ permutations of $\sigma_y^{\otimes n}$, e.g., for $N = 4$ and $n = 2$, these are $\sigma_y \otimes \sigma_y \otimes I \otimes I$, $\sigma_y \otimes I \otimes \sigma_y \otimes I$, ... Figure 5 shows the rescaled $\tilde{\tau}_{n,N}$ for different values of N and n. These quantities are seen to exhibit convergence to a fixed curve with increasing N, starting for relatively small system sizes. The time required to reach the plateau region increases with n, consistent with the notion that more time is required to entangle n neutrinos than $n - 1$. Moreover, upon further investigation, these plateaus are found to be robust against variations of the two-body coupling strength (increasing or decreasing the angle of the cone) and vacuum-mixing angle (more or less oscillatory behavior), the only observed difference is in the relaxation time (shorter times for wider cones because the interaction strength J_{ij} is stronger).

While this scaling is somewhat puzzling, it can be compared to other entangled multiqubit systems, for which analytic results are available. For example, the GHZ state has $\tau_{n=N} = 1$ and $\tau_{n<N} = 0$, while the W state has $\tau_n = 0\ \forall\ n$ except for $\tau_{n=2} = 2(N-1)/N$ (with $\tau_n = \sum_i \tau_n^{(i)}$ for $n < N$). A system that has similar scaling is the product

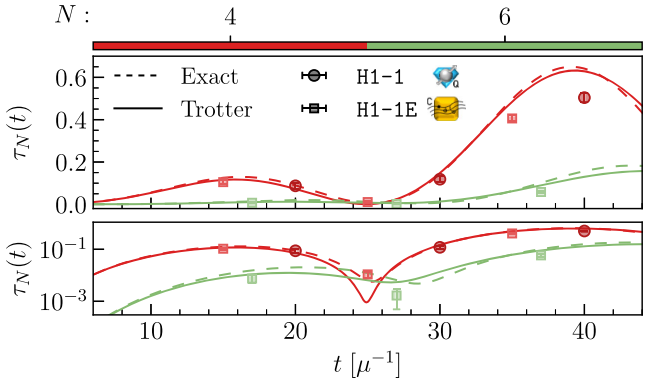

FIG. 4. N-tangle τ_N for $N = \{4, 6\}$ neutrinos on a linear (top) and log (bottom) scale. The lines show the Trotter (continuous) or exact (dashed) simulation, and the points show the results from `H1-1` (dark circles, using 480 shots) and `H1-1E` (light squares, using 1200 shots).

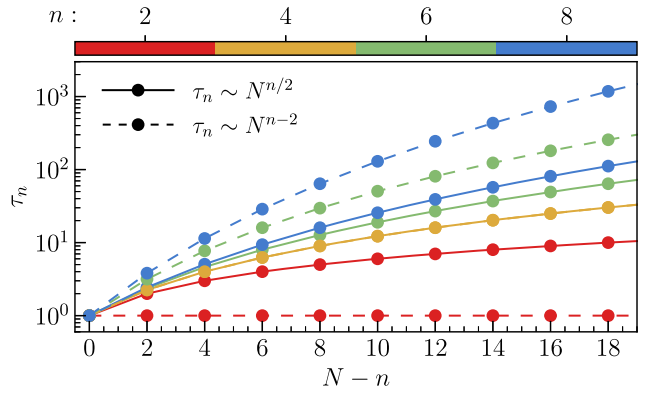

FIG. 6. Comparison of two scalings of the n-tangles, $N^{n/2}$ (continuous line) as found for systems of Bell pairs, and N^{n-2} (dashed line) as we have identified from the time evolution, for different values of n and system sizes N, normalized to $\tau_{n=N} = 1$.

of $N/2$ Bell pairs, with $\tau_n = \binom{N/2}{N/2-n/2} \sim N^{n/2}$. Comparing this with the scaling from Eq. (11), the n-tangle grows faster for the neutrino state than the Bell-pairs state with system size (except for τ_2 and τ_4), as depicted in Fig. 6. This implies that there is multi-neutrino entanglement, beyond the two-neutrino entanglement found in the $(N/2)$-product Bell-pairs state.

The present analysis concerns the coherent flavor oscillations of a mono-energetic neutrino gas starting in a mixed-flavor pure state. To gain an understanding of such dynamics in a mixed state, we have also examined the impact of different initial states for the evolution, and find that the values of n-tangle depend upon the initial state in nontrivial ways. A monoflavor initial state gives vanishing n-tangle, while an initial state with a single distinct flavor has nonzero 2-tangle, resembling a W-state (the oscillations are too large to discriminate between the different N scalings, consistent with $2(N-1)/N$ or N^{n-2}). Gases of different energy neutrinos can be described within this framework through different values of $\mathbf{b}$ in Eq. (2).

Summary and conclusions.—The time evolution of multi-neutrino quantum correlations and entanglement in dense neutrino systems is studied for systems of $N = 4$, 6, 8, and 12 neutrinos using Quantinuum's `H1-1` 20 qubit trapped ion quantum computer and its associated noisy emulator `H1-1E`. The central reason for including and developing methods for implementation on quantum computers is that determining the entanglement of the larger systems that will be required as input into realistic astrophysical simulations will need quantum simulations of such systems with larger numbers of neutrinos (than in this work). We have chosen to study the n-tangle in order to provide insight into the multiparticle entanglement structure of the systems. Compared to other entanglement witnesses, the n-tangle is straightforward to compute using a quantum computer (at least for a single product state, as considered here), since it does not require state tomography. The behavior of rescaled sums over n-tangles are found to converge to universal curves with increasing system sizes, that depend upon the parameters of the Hamiltonian, with late-time plateaus. Further, the magnitudes of the n-tangles are found to increasingly exceed that of systems comprised of neutrino Bell pairs, indicating the presence of genuine multi-neutrino entanglement in collective coherent neutrino flavor oscillations in dense systems.

We would like to thank Valentina Amitrano, Ramya Bhaskar, Joe Carlson, Anthony Ciavarella, Roland Farrell, Francesco Pederiva, Alessandro Roggero, and Francesco Turro, along with the QSC Thrust-2 team, for insightful discussions. This work was supported in part by the U.S. Department of Energy, Office of Science, Office of Nuclear Physics, InQubator for Quantum Simulation (IQuS) [73] under Award No. DOE (NP) Award No. DE-SC0020970 (Savage), and the Quantum Science Center (QSC) [74], a National Quantum Information Science Research Center of the U.S. Department of Energy (DOE) (Illa). This work is also supported, in part, through the Department of Physics [75] and the College of Arts and Sciences [76] at the University of Washington. This research used resources of the Oak Ridge Leadership Computing Facility, which is a DOE Office of Science User Facility supported under Contract No. DE-AC05-00OR22725. We have made extensive use of Wolfram *Mathematica* [77], PYTHON [78,79], and JUPYTER Notebooks [80] in the CONDA environment [81], JULIA [82–84] and the quantum programming environments: IBM's QISKIT [85] and CQC's PYTKET [60].

*marcilla@uw.edu
†mjs5@uw.edu

[1] H. Duan and J. P. Kneller, Neutrino flavour transformation in supernovae, J. Phys. G **36**, 113201 (2009).
[2] H. Duan, G. M. Fuller, and Y.-Z. Qian, Collective neutrino oscillations, Annu. Rev. Nucl. Part. Sci. **60**, 569 (2010).
[3] S. Chakraborty, R. Hansen, I. Izaguirre, and G. Raffelt, Collective neutrino flavor conversion: Recent developments, Nucl. Phys. **B908**, 366 (2016).
[4] I. Tamborra and S. Shalgar, New developments in flavor evolution of a dense neutrino gas, Annu. Rev. Nucl. Part. Sci. **71**, 165 (2021).
[5] F. Capozzi and N. Saviano, Neutrino flavor conversions in high-density astrophysical and cosmological environments, Universe **8**, 94 (2022).
[6] G. M. Fuller, R. W. Mayle, J. R. Wilson, and D. N. Schramm, Resonant neutrino oscillations and stellar collapse, Astrophys. J. **322**, 795 (1987).
[7] M. J. Savage, R. A. Malaney, and G. M. Fuller, Neutrino oscillations and the leptonic charge of the Universe, Astrophys. J. **368**, 1 (1991).
[8] J. Pantaleone, Dirac neutrinos in dense matter, Phys. Rev. D **46**, 510 (1992).
[9] J. Pantaleone, Neutrino oscillations at high densities, Phys. Lett. B **287**, 128 (1992).
[10] B. H. J. McKellar and M. J. Thomson, Oscillating neutrinos in the early Universe, Phys. Rev. D **49**, 2710 (1994).
[11] N. F. Bell, A. A. Rawlinson, and R. F. Sawyer, Speedup through entanglement: Many body effects in neutrino processes, Phys. Lett. B **573**, 86 (2003).
[12] A. Friedland and C. Lunardini, Do many particle neutrino interactions cause a novel coherent effect?, J. High Energy Phys. 10 (2003) 043.
[13] R. F. Sawyer, "Classical" instabilities and "quantum" speedup in the evolution of neutrino clouds, arXiv:hep-ph/0408265.
[14] Y. Pehlivan, A. B. Balantekin, T. Kajino, and T. Yoshida, Invariants of collective neutrino oscillations, Phys. Rev. D **84**, 065008 (2011).
[15] E. Rrapaj, Exact solution of multiangle quantum many-body collective neutrino-flavor oscillations, Phys. Rev. C **101**, 065805 (2020).
[16] M. J. Cervia, A. V. Patwardhan, A. B. Balantekin, S. N. Coppersmith, and C. W. Johnson, Entanglement and

collective flavor oscillations in a dense neutrino gas, Phys. Rev. D **100**, 083001 (2019).
[17] A. Roggero, Entanglement and many-body effects in collective neutrino oscillations, Phys. Rev. D **104**, 103016 (2021).
[18] B. Hall, A. Roggero, A. Baroni, and J. Carlson, Simulation of collective neutrino oscillations on a quantum computer, Phys. Rev. D **104**, 063009 (2021).
[19] A. Roggero, Dynamical phase transitions in models of collective neutrino oscillations, Phys. Rev. D **104**, 123023 (2021).
[20] K. Yeter-Aydeniz, S. Bangar, G. Siopsis, and R. C. Pooser, Collective neutrino oscillations on a quantum computer, Quantum Inf. Process. **21**, 84 (2022).
[21] A. V. Patwardhan, M. J. Cervia, and A. B. Balantekin, Spectral splits and entanglement entropy in collective neutrino oscillations, Phys. Rev. D **104**, 123035 (2021).
[22] Z. Xiong, Many-body effects of collective neutrino oscillations, Phys. Rev. D **105**, 103002 (2022).
[23] J. D. Martin, A. Roggero, H. Duan, J. Carlson, and V. Cirigliano, Classical and quantum evolution in a simple coherent neutrino problem, Phys. Rev. D **105**, 083020 (2022).
[24] M. J. Cervia, P. Siwach, A. V. Patwardhan, A. B. Balantekin, S. N. Coppersmith, and C. W. Johnson, Collective neutrino oscillations with tensor networks using a time-dependent variational principle, Phys. Rev. D **105**, 123025 (2022).
[25] M. Illa and M. J. Savage, Basic elements for simulations of standard-model physics with quantum annealers: Multigrid and clock states, Phys. Rev. A **106**, 052605 (2022).
[26] A. Roggero, E. Rrapaj, and Z. Xiong, Entanglement and correlations in fast collective neutrino flavor oscillations, Phys. Rev. D **106**, 043022 (2022).
[27] D. Lacroix, A. B. Balantekin, M. J. Cervia, A. V. Patwardhan, and P. Siwach, Role of non-Gaussian quantum fluctuations in neutrino entanglement, Phys. Rev. D **106**, 123006 (2022).
[28] V. Amitrano, A. Roggero, P. Luchi, F. Turro, L. Vespucci, and F. Pederiva, Trapped-ion quantum simulation of collective neutrino oscillations, Phys. Rev. D **107**, 023007 (2023).
[29] A. Wong and N. Christensen, Potential multiparticle entanglement measure, Phys. Rev. A **63**, 044301 (2001).
[30] Quantinuum (2022), https://www.quantinuum.com/.
[31] B. Pontecorvo, Mesonium and anti-mesonium, Sov. Phys. JETP **6**, 429 (1957).
[32] B. Pontecorvo, Inverse beta processes and nonconservation of lepton charge, Sov. Phys. JETP **7**, 172 (1958).
[33] Z. Maki, M. Nakagawa, and S. Sakata, Remarks on the unified model of elementary particles, Prog. Theor. Phys. **28**, 870 (1962).
[34] B. Pontecorvo, Neutrino experiments and the problem of conservation of leptonic charge, Sov. Phys. JETP **26**, 984 (1968).
[35] L. Wolfenstein, Neutrino oscillations in matter, Phys. Rev. D **17**, 2369 (1978).
[36] S. P. Mikheyev and A. Y. Smirnov, Resonance amplification of oscillations in matter and spectroscopy of solar neutrinos, Sov. J. Nucl. Phys. **42**, 913 (1985).
[37] I. Esteban, M. C. Gonzalez-Garcia, M. Maltoni, T. Schwetz, and A. Zhou, The fate of hints: Updated global analysis of three-flavor neutrino oscillations, J. High Energy Phys. 09 (2020) 178.
[38] A. B. Balantekin and G. M. Fuller, Constraints on neutrino mixing, Phys. Lett. B **471**, 195 (1999).
[39] H.-Y. Huang, R. Kueng, and J. Preskill, Predicting many properties of a quantum system from very few measurements, Nat. Phys. **16**, 1050 (2020).
[40] S. A. Hill and W. K. Wootters, Entanglement of a Pair of Quantum Bits, Phys. Rev. Lett. **78**, 5022 (1997).
[41] W. K. Wootters, Entanglement of Formation of an Arbitrary State of Two Qubits, Phys. Rev. Lett. **80**, 2245 (1998).
[42] V. Coffman, J. Kundu, and W. K. Wootters, Distributed entanglement, Phys. Rev. A **61**, 052306 (2000).
[43] X. Li and D. Li, Relationship between the n-tangle and the residual entanglement of even n qubits, Quantum Inf. Comput. **10**, 1018 (2010).
[44] D. M. Greenberger, M. A. Horne, and A. Zeilinger, Going beyond Bell's theorem, in *Bell's Theorem, Quantum Theory and Conceptions of the Universe* (Springer, New York, 1989), pp. 69–72, arXiv:0712.0921.
[45] D. Bouwmeester, J.-W. Pan, M. Daniell, H. Weinfurter, and A. Zeilinger, Observation of Three Photon Greenberger-Horne-Zeilinger Entanglement, Phys. Rev. Lett. **82**, 1345 (1999).
[46] W. Dur, G. Vidal, and J. I. Cirac, Three qubits can be entangled in two inequivalent ways, Phys. Rev. A **62**, 062314 (2000).
[47] There are other ways to ascertain the nature of entanglement in these systems. For example, a more complete set of two-point correlation functions could be used to determine the Quantum Fisher information, $F = \sum_{\alpha,\beta} \sum_{i,j} n^i_\alpha C^{i,j}_{\alpha,\beta} n^j_\beta$, with n^i_α being unit vectors and $C^{i,j}_{\alpha,\beta} = \langle \sigma^{(i)}_\alpha \sigma^{(j)}_\beta \rangle - \langle \sigma^{(i)}_\alpha \rangle \langle \sigma^{(j)}_\beta \rangle$, which can be used to learn about the nature of entanglement [48,49].
[48] P. Hyllus, W. Laskowski, R. Krischek, C. Schwemmer, W. Wieczorek, H. Weinfurter, L. Pezzé, and A. Smerzi, Fisher information and multiparticle entanglement, Phys. Rev. A **85**, 022321 (2012).
[49] G. Tóth, Multipartite entanglement and high-precision metrology, Phys. Rev. A **85**, 022322 (2012).
[50] R. C. Farrell, I. A. Chernyshev, S. J. M. Powell, N. A. Zemlevskiy, M. Illa, and M. J. Savage, Preparations for quantum simulations of quantum chromodynamics in $1 + 1$ dimensions. II. Single-baryon β-decay in real time, Phys. Rev. D **107**, 054513 (2023).
[51] A. Barenco, C. H. Bennett, R. Cleve, D. P. DiVincenzo, N. Margolus, P. Shor, T. Sleator, J. A. Smolin, and H. Weinfurter, Elementary gates for quantum computation, Phys. Rev. A **52**, 3457 (1995).
[52] F. Vatan and C. Williams, Optimal quantum circuits for general two-qubit gates, Phys. Rev. A **69**, 032315 (2004).
[53] G. Vidal and C. M. Dawson, Universal quantum circuit for two-qubit transformations with three controlled-NOT gates, Phys. Rev. A **69**, 010301(R) (2004).
[54] M. W. Coffey, R. Deiotte, and T. Semi, Comment on "Universal quantum circuit for two-qubit transformations with three controlled-NOT gates" and "Recognizing

small-circuit structure in two-qubit operators", Phys. Rev. A **77**, 066301 (2008).

[55] Following Ref. [56], and assuming no additional ancilla qubits are used, for general single-qubit rotations U_1, Refs. [57,58] give the following estimates of the number of T gates, $T_{U1}(\epsilon) = 2.95\log_2(1/\epsilon) + 3.75$. For R_z, Ref. [59] gives $T_{Rz}(\epsilon) = 3.21\log_2(1/\epsilon) - 6.93$.

[56] A. Paetznick and K. M. Svore, Repeat-until-success: Non-deterministic decomposition of single-qubit unitaries, Quantum Inf. Comput. **14**, 1277 (2014).

[57] A. G. Fowler, Constructing arbitrary Steane code single logical qubit fault-tolerant gates, Quantum Inf. Comput. **11**, 867 (2011).

[58] A. Bocharov and K. M. Svore, Resource-Optimal Single-Qubit Quantum Circuits, Phys. Rev. Lett. **109**, 190501 (2012).

[59] V. Kliuchnikov, D. Maslov, and M. Mosca, Practical approximation of single-qubit unitaries by single-qubit quantum Clifford and T circuits, IEEE Trans. Comput. **65**, 161 (2016).

[60] S. Sivarajah, S. Dilkes, A. Cowtan, W. Simmons, A. Edgington, and R. Duncan, t|ket⟩: A retargetable compiler for NISQ devices, Quantum Sci. Technol. **6**, 014003 (2020).

[61] C. Cîrstoiu, Z. Holmes, J. Iosue, L. Cincio, P. J. Coles, and A. Sornborger, Variational fast forwarding for quantum simulation beyond the coherence time, npj Quantum Inf. **6**, 82 (2020).

[62] N. Klco and M. J. Savage, Minimally entangled state preparation of localized wave functions on quantum computers, Phys. Rev. A **102**, 012612 (2020).

[63] See Supplemental Material at http://link.aps.org/supplemental/10.1103/PhysRevLett.130.221003 for additional figures and tabulated data from the quantum simulations.

[64] J. J. Wallman and J. Emerson, Noise tailoring for scalable quantum computation via randomized compiling, Phys. Rev. A **94**, 052325 (2016).

[65] M. Urbanek, B. Nachman, V. R. Pascuzzi, A. He, C. W. Bauer, and W. A. de Jong, Mitigating Depolarizing Noise on Quantum Computers with Noise-Estimation Circuits, Phys. Rev. Lett. **127**, 270502 (2021).

[66] S. A Rahman, R. Lewis, E. Mendicelli, and S. Powell, Self-mitigating Trotter circuits for SU(2) lattice gauge theory on a quantum computer, Phys. Rev. D **106**, 074502 (2022).

[67] R. C. Farrell, I. A. Chernyshev, S. J. M. Powell, N. A. Zemlevskiy, M. Illa, and M. J. Savage, Preparations for quantum simulations of quantum chromodynamics in $1 + 1$ dimensions. I. Axial gauge, Phys. Rev. D **107**, 054512 (2023).

[68] N. Klco, M. J. Savage, and J. R. Stryker, SU(2) non-Abelian gauge field theory in one dimension on digital quantum computers, Phys. Rev. D **101**, 074512 (2020).

[69] N. H. Nguyen, M. C. Tran, Y. Zhu, A. M. Green, C. H. Alderete, Z. Davoudi, and N. M. Linke, Digital quantum simulation of the Schwinger model and symmetry protection with trapped ions, PRX Quantum **3**, 020324 (2022).

[70] A. Barenco, A. Berthiaume, D. Deutsch, A. Ekert, R. Jozsa, and C. Macchiavello, Stabilization of quantum computations by symmetrization, SIAM J. Comput. **26**, 1541 (1997).

[71] H. Buhrman, R. Cleve, J. Watrous, and R. de Wolf, Quantum Fingerprinting, Phys. Rev. Lett. **87**, 167902 (2001).

[72] J. L. Beckey, N. Gigena, P. J. Coles, and M. Cerezo, Computable and Operationally Meaningful Multipartite Entanglement Measures, Phys. Rev. Lett. **127**, 140501 (2021).

[73] https://iqus.uw.edu.

[74] https://qscience.org.

[75] https://phys.washington.edu.

[76] https://www.artsci.washington.edu.

[77] Wolfram Research, Inc., *Mathematica*, Version 13.0.1 (2022), Champaign, IL, https://www.wolfram.com/mathematica.

[78] G. Van Rossum and F. L. Drake, *PYTHON 3 Reference Manual* (CreateSpace, Scotts Valley, CA, 2009).

[79] J. D. Hunter, MATPLOTLIB: A 2D graphics environment, Comput. Sci. Eng. **9**, 90 (2007).

[80] F. Pérez and B. E. Granger, IPYTHON: A System for Interactive Scientific Computing, Comput. Sci. Eng. **9**, 21 (2007).

[81] Anaconda Inc., Anaconda Software Distribution, Vers. 2-2.4.0 (2020), https://docs.anaconda.com/.

[82] J. Bezanson, A. Edelman, S. Karpinski, and V. B. Shah, JULIA: A fresh approach to numerical computing, SIAM Rev. **59**, 65 (2017).

[83] A. Croy *et al.*, EXPOKIT.JL: JULIA implementations of EXPOKIT (2018), https://github.com/acroy/Expokit.jl.

[84] R. B. Sidje, EXPOKIT: A software package for computing matrix exponentials, ACM Trans. Math. Softw. **24**, 130 (1998).

[85] M. Treinish *et al.*, QISKIT/QISKIT: QISKIT 0.36.2 (2022), 10.5281/zenodo.6560959.